Personality effects on spatial learning: comparisons between visual conditions in a weakly-electric fish

Kareklas, Kyriacos; Elwood, Robert W.; Holland, Richard

Ethology

DOI:
10.1111/eth.12629

Published: 01/01/2017

Peer reviewed version

Effect of digital acquisition on complexity of chaos

Hong, Yanhua; Ji, Songkun

Optics Letters

Accepted/In press: 05/06/2017

Effect of digital acquisition on complexity of chaos

YANHUA HONG*, SONGKUN JI

School of Electronic Engineering, Bangor University, Gwynedd LL57 1UT, Wales, UK
**Corresponding author: y.hong@bangor.ac.uk*

Received 24 April 2017; revised 25 May 2017; accepted 02 June 2017

Effect of data acquisition on the complexity of chaos using permutation entropy has been studied experimentally and numerically. The complexity of chaos is quantified using the normalized permutation entropy at the feedback round trip time. Two 'abnormal' variations of complexity of chaos with bias current have been observed experimentally. The different vertical scales of the oscilloscope in data acquisition are attributed to this 'abnormal' change. The method to remove the effect of data acquisition has also been proposed. © 2017 Optical Society of America

OCIS codes: *(140.1540) Chaos; (140.5960) Semiconductor lasers, (120.3940) Metrology; (120.1880) Detection.*

http://dx.doi.org/10.1364/OL.99.099999

Chaos generated in semiconductor lasers with time-delayed optical feedback has attracted great research interest because of many potential applications of chaos [1-14], such as high-speed chaotic optical communications, chaotic optical time-domain reflectors, chaotic lidar, physical random number generators and chaos computing. The complexity of chaos is one of the important parameters for assessing the suitability of chaos for its applications. Several techniques have been used to quantify the complexity of chaos, such as Lyapunov exponents [15–16], strangeness of strange attractors [17] and permutation entropy (PE) [18–24]. PE is a method based on the relative amplitude of time series value. The advantages for using PE as a quantifier to measure the relative complexity are easy implementation, faster computation and being robust to noise. This makes PE particularly attractive on analyzing experimental chaotic data. However, the value of PE can be affected by many factors, such as, the selection of subset dimension in the calculation, the sample rate, delay time and the total number of points in the time series [19-21]. The minimum required sampling rate to capture all the information of the fast chaotic dynamics decreases when the embedding dimension increases [19]. A brief description of the effect of the acquisition conditions on random bit generation has also been reported [25-26]. Using the value of PE at the delayed time equal to the external cavity round trip time to quantify the complexity of chaos agrees with the definition of weak or strong chaos [20]. In this letter, we also adopted the complexity of chaos being quantified using the value of PE at feedback round trip time. We observed two 'abnormal' variations of complexity with bias current. This phenomenon, to the best of our knowledge, has not been reported and investigated. We use both experimental and numerical methods to analyze this 'abnormal' phenomenon. We also provide a method to remove this 'abnormal' condition.

Figure 1 shows the schematic of the experimental setup. A laser from Eblana Photonics with lasing wavelength around 1.55μm was used in the experiment. The laser was driven by an ultra-low noise current source and its temperature was controlled to an accuracy of 0.01 ^{0}C. At the setting temperature in the experiment, the threshold current was 14.7mA. The laser was subject to optical feedback through the fiber loop and the feedback round trip time was 42.6ns. The polarization controller (PC) in the fiber loop was used to adjust the polarization of the feedback beam to make it parallel to the polarization of the free-running laser. The feedback ratio was -14.3 dB and the laser was rendered chaotic in all the operating bias currents. The feedback ratio is defined as the ratio of the optical feedback power to the laser's free-running output power. The optical feedback power was measured at port 2 of the optical circulator (Cir) before it was fed back into the laser.

The output of the laser was connected to a digital fiber attenuation (ATTN), detected by a 12 GHz bandwidth photodetector (D) and recorded by a 4 GHz bandwidth digital oscilloscope (OSC). The vertical resolution of the oscilloscope was 8 bits. The sampling rate of the oscilloscope was set at 10 GS/s with 100000 samples recorded for each time trace, therefore the duration of each time trace was 10 μs.

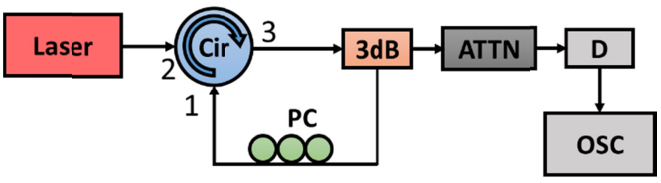

Fig. 1. The experimental Setup. Cir-optical circulator; 3dB-3dB optical coupler; PC-polarization controller; ATTN-optical attenuator; D-photodetector; OSC-digital oscilloscope.

Fig. 2 (a) shows the time traces of chaos generated in the laser diode. The grey (red for online version) line is noise floor from the stable operation laser. The output of the laser shows large

amplitude fluctuation, which indicates that the laser was operating in a chaotic region. The normalized PE (H(P)) as a function of embedding delay time was calculated and displayed in Fig. 2(b). The details of the normalized PE definition can be found in references [18-24]. The value of the normalised PE is between 0 and 1 [20]. A value of one represents a completely stochastic process, while a value of zero indicates that the time series is completely predictable. The length of the ordinal pattern in this paper was chosen as 4. It is obvious that there are troughs around the feedback round trip time (τ_{ext}) of 42.6 ns and its subharmonics. As indicated in the introduction, this trough value at the feedback round time can be used to measue the complexity of choas [20, 24], and we adopt it to characterize the complexity of chaos. It is noted that the trough may not be located exactly at τ_{ext} [24]. If a measured trough value is in the range of interval of ($\tau_{ext} - \tau_{ext} \times r_1$, $\tau_{ext} + \tau_{ext} \times r_1$), it will be considered as the trough at τ_{ext}. According to the experimental data, 2% is selected as the value of r_1.

Fig. 3 shows the complexity of chaotic signals as a function of the laser bias current. For bias currents above 23 mA, the complexity is almost constant and varies smoothly . However, at lower bias currents, there are two 'abnormal' areas, where the complexity drops abruptly when the bias current increases both from 17.5 mA to 18 mA and from 20.5 mA to 21 mA, respectively. In order to investigate these 'abnormal' phenomena, the data acquisition condition was checked carefully. We found that the fluctuation amplitude increases with the increasing bias current. At the 'abnormal' regions, the vertical scale of the oscilloscope was increased to prevent high amplitudes from being saturated.

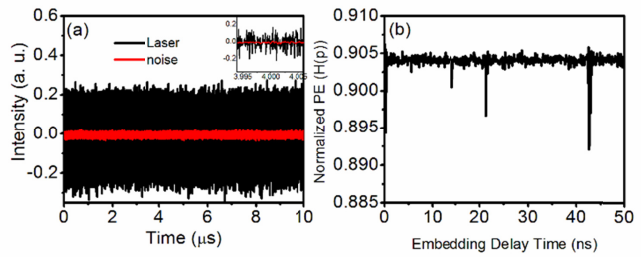

Fig. 2. (a) The time trace of the laser output and (b) the normalized PE as a function of embedding delay time. The inset in Fig. 2(a) is the time series in a shorter time interval.

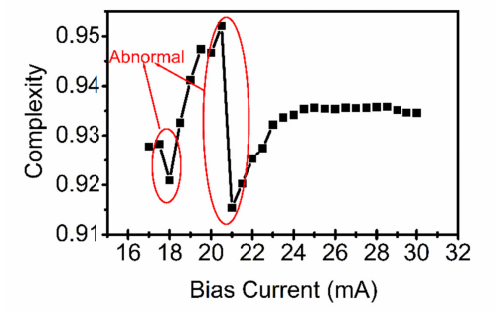

Fig. 3. The complexity of the chaotic signal as a function of bias current.

In order to prevent the change of the vertical scale of the oscilloscope, two approaches were adopted to record the data. Firstly, the output of the laser was coupled into the detector without changing the attenuation and the vertical scale of the oscilloscope. The vertical scale was set in such a way that the maximum fluctuation amplitude would not exceed the scale of the oscilloscope. The complexity of chaos with the increasing bias current was calculated, and the result is shown in fig. 4(a). The result shows that the complexity of chaos is almost monotonically increasing with increasing bias current. The sudden drop of complexity has not been observed. In the second method of data acquisition, the vertical scale of the oscilloscope was kept unchanged, but the amplitude of the signal was adjusted by an optical attenuator to ensure the amplitude of the signal can use the full-8-bit vertical resolution range of the oscilloscope. Under this data acquisition condition, the results obtained are illustrated in Fig.4 (b). We can see the complexity increases with the increasing bias current for lower bias currents (< 22 mA). When the bias current is above 22 mA, the complexity shows saturation, and the bias current has little effect on the complexity. The two 'abnormal' variations of the complexity have also disappeared.

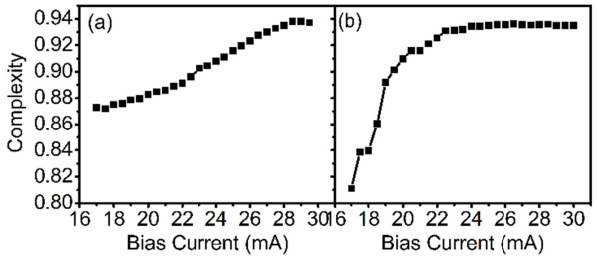

Fig. 4. The complexity of the chaotic signal as a function of bias current under a fixed vertical scale of the oscilloscope. (a) No optical attenuator before the detector, (b) with optical attenuator before the detector.

From the above results, we can see that three different results were obtained when the three different data acquisition methods were used. In order to identify which results are the true characteristics of chaos, chaos generated in semiconductor lasers with optical feedback have been numerically simulated using the Lang Kobayashi laser equations [27], as shown in Eqs (1) and (2) below.

$$\frac{dE}{dt} = \frac{1}{2}(1+i\alpha)\left[G - \frac{1}{\tau_p}\right]E(t) + \kappa E(t-\tau_{ext})e^{-i\omega\tau_{ext}} \quad (1)$$

$$\frac{dN}{dt} = \frac{I}{eV} - \frac{N(t)}{\tau_N} - G|E(t)|^2 \quad (2)$$

In the rate equations, E(t) is the complex electric field, N(t) is the carrier number. α is the line-width enhanced factor, κ is the feedback strength, τ_p is the photon lifetime, τ_N is the carrier lifetime, τ_{ext} is the external cavity round-trip time, ω is the angular frequency of the laser, V is the volume of the active region, e is the electron charge and I is the laser bias current. The optical gain G is given by

$$G = g_0(N - N_0)\frac{1}{1+\epsilon|E(t)|^2} \quad (3)$$

where g_0 is the differential gain, ϵ is the gain saturation factor, and N_0 is the carrier density at transparency.

In the simulation, the following parameter values are chosen: α=3, τ_p = 2ps, τ_N =2ns, ω =1.216×10^{15} rad/s (which correspond to a lasing wavelength of 1.55 μm), V = 1.225×10^{-16} m^3,g_0 = 5.0×10^{-12} m^{3}s^{-1}, ϵ = 5.0×10^{-23} and N_0 = 1.4×10^{24} m^{-3}. From these parameters, the laser's threshold current is 14.7 mA, which is the same as the threshold current of the laser we used in the experiment. The relaxation oscillation frequencies for the bias currents above 1.1 times threshold current are more than 3 GHz, so the feedback round trip time of more than 0.34 ns is considered to be long-cavity feedback case [28]. Our recent work has also shown that the feedback round trip time has little effect on the trend of complexity for long cavity feedback [29]. In order to save the simulation time, 1ns is taken for τ_{ext}. According to the relationship between feedback ratio measured in the experiment and the feedback strength in the simulation [30], κ= 40ns^{-1} is selected to represent the feedback ratio in the experiment. At this feedback strength, the time series is similar to that in Fig. 2(a), where the laser operates at chaotic dynamics. The complexity of the laser chaotic output has been analyzed using the time series calculated from the above rate equations with a temporal resolution of Δt of 10 ps and the result is shown in Fig. 5. The curve clearly shows that the complexity increases in line with the bias current for bias currents below 23 mA. When the bias currents are above 23mA, slight variation of the complexity with the bias current have been displayed with no trend towards one way or another. This result is qualitative in good agreement with the experimental result showed in Fig. 4(b).

Effect of the vertical resolution of the oscilloscope on the value of the complexity is further analysed. A time series calculated from the rate equations with the bias current of 25 mA was used. Fig. 6(a) shows the complexity obtained from this time series. The result shows that the value of the complexity is close to 1 for most of the embedding delay time except at the feedback round trip time of 1ns and its sub-harmonics. When the data is recorded in an oscilloscope in the experiment, the analogue chaotic signal is converted into a digital signal. Currently, the common vertical resolution of the oscilloscope is 8-bit. If the amplitude of chaos signal covers the full 8-bit range of the oscilloscope, the chaotic signal will be digitized to 255 (2^8-1) levels between the maximum and minimum amplitude. In Fig. 6(b), we calculate the complexity from the same time series used in Fig. 6(a), but the data has been digitized to 255 levels. It is noted that the variation trend of the normalized PE with the embedding delay time is the same as that in Fig. 6(a), but all its values have been reduced by 3%. In the experiment, the vertical-scale may need to be changed to avoid the amplitude of the chaotic signal being saturated. Here we can consider a simple case, where the maximum amplitude is about to exceed the full 8-bit range of the oscilloscope and the vertical scale of the oscilloscope is increased by a factor of 2. In such a case, the values between the maximum and minimum can be digitized to 127 (2^7-1) levels. Fig. 6(c) shows the calculation result, where the same time series in Fig. 6(a) is digitized to 127 levels instead of 255 levels. We can see a similar trend of the normalized PE as a function of embedding delay time achieved, but with the absolute values further reduced by another 3%. This result explains why the complexity decreases dramatically at the bias currents between 18mA and 21 mA when the vertical scale of the oscilloscope is increased in the experiment.

For 6(d), the amplitude of the time series used in Fig. 6(a) is reduced to its half value, but this time series is still digitized to 255 levels. This is similar to the case that the vertical scale of the oscilloscope is adjusted to guarantee the signal takes up the full 8-bit range but without surpassing it when an optical attenuator is used to reduce the signal power. The complexity of this time series is calculated. We can see that the result is the same as that in Fig. 6(b). This indicates that the absolute power would not influence the normalized PE value, but the data's digitization will affect its results. The reason for this phenomenon is that PE is a method based on the relative amplitude of time series value, not the absolute value.

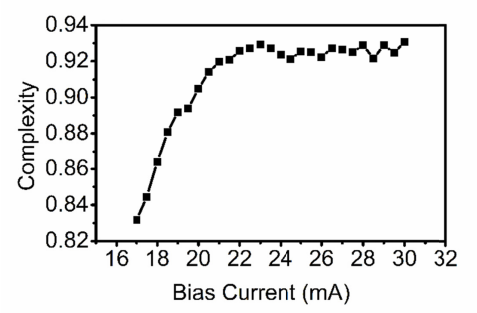

Fig. 5. Numerical simulation of the complexity as a function of bias current.

Two minima separated by half reciprocal the relaxation oscillation frequency (1/(2f_{RO})) near τ_{ext} [19, 24] are not obvious in Fig.6 and Fig.2(b). It may due to lower bandwidth (4GHz) oscilloscope for Fig. 2(b). Lower bandwidth oscilloscope causes the loss of the dynamics at frequencies close to f_{RO}. For the simulation results in Fig. 6, lower length of the ordinal pattern for PE calculation may be attribute to less significant of the signature of f_{RO}. It is interesting to see that the signature of f_{RO} near τ_{ext} becomes clearer for less digitized levels, as indicated by an arrow in Fig. 6(c). This phenomenon is outside the scope of this paper and will be investigated in the future study. Fig. 6 also shows that the maximum normalised PE value (the "flat" value) decreases with decreased digitisation levels, whereas the trough depth of the normalized PE at τ_{ext} increases at the same time.

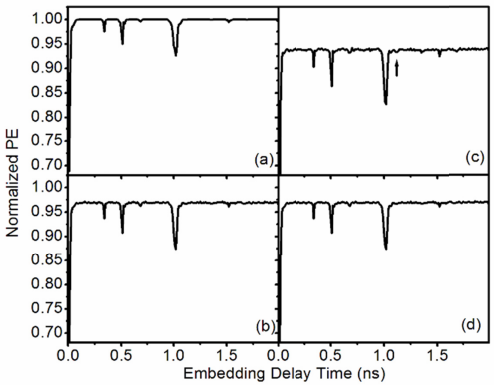

Fig. 6. The normalized PE calculated from (a) the time series calculated from the rate equations; (b) the time series being digitized to 255 levels; (c) the time series being digitized to 127 levels; (d) the time series whose amplitude has been reduced by half and digitized to 255 levels.

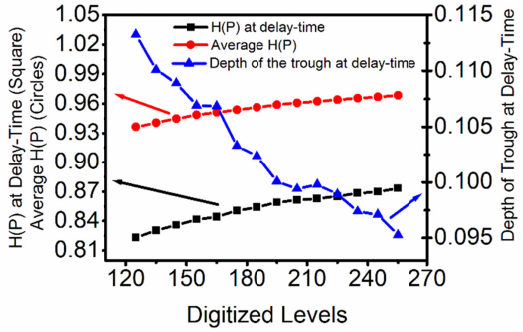

Fig. 7. Numerical simulation effect of the digitized levels on the average normalized PE (circles), the normalized PE at τ_{ext} (squares) and the depth of the trough at τ_{ext} (triangles) as a function of digitized levels.

To better show the effect of digital acquisition on the normalized PE, the normalized PE at τ_{ext}, the average normalized PE and the trough depth at τ_{ext} of the time series used in Fig. 6(a)) as a function of digitized levels are plotted in Fig. 7. This is analogous to the scenario that the same time series is being recorded by an oscilloscope using a different vertical scale. The average PE is the average value of the normalized PE for the embedding delay time between 1.2ns and 1.4ns, which corresponds to the maximum normalised PE value (the "flat" value). The trough depth at τ_{ext} is defined as the difference between the average normalized PE and the normalized PE at τ_{ext}. The result exhibits that both the normalized PE at τ_{ext}, and the average normalized PE increase monotonically with increased digitized levels, but the increase rate for the normalized PE at τ_{ext} is slightly faster than that of the average normalized PE, therefore the trough depth at τ_{ext} decreases with the increased digitized levels. The results in Fig. 7 prove that the data acquisition should cover the full vertical resolution of the oscilloscope to reduce the degradation of the complexity of chaos signal, as recommended in [25-26]. For the comparison of complexity of chaos using PE, all data should use the same digitized levels.

In conclusion, effect of data acquisition on the complexity using permutation entropy has been studied experimentally and theoretically. Two 'abnormal' variations of complexity of chaos with bias current observed in the experiment can be attributed to the change of data digitization resolution. The complexity increases with increased digitized levels. In order to reduce the degradation of the complexity of chaos signal, the data acquisition should cover the full vertical resolution of the oscilloscope. For the comparison of complexity of chaos using PE, all data should be acquired using the same resolution of the digitization.

Funding. The Sêr Cymru National Research Network in Advanced Engineering and Materials (NRN158); International cooperation project of key research and development plan of Shanxi Province, China (201603D421008).

Acknowledgment. We thank Prof Yuncai Wang and Prof. Anbang Wang from Key Laboratory of Advanced Transducers and Intelligent Control System, Ministry of Education, College of Physics and Optoelectronics, Taiyuan University of Technology, China for their very useful comments and advices.

References

1. C. Masoller, Phys. Rev. Lett., **86**, 2782 (2001).
2. Y. Takiguchi, K. Ohyagi and J. Ohtsubo, Opt. Lett., **28**, 319 (2003).
3. Y. Hong, M. W. Lee, P. S. Spencer and K. A. Shore, Opt. Lett., **29**, 1215 (2004).
4. F.-Y. Lin and J.-M. Liu, IEEE J. Sel. Top. quantum Electron., **10**, 991 (2004).
5. A. Argyris, D. Syvridis, L. Larger, V. Annovazzi-Lodi, P. Colet, I. Fischer, J. García-Ojalvo, C. R. Mirasso, L. Pesquera, and K. A. Shore, Nature, **438**, 343 (2005).
6. A. Uchida, K. Amano, M. Inoue, K. Hirano, S. Naito, H. Someya, I. Oowada, T. Kurashige, M. Shiki, S. Yoshimori, K. Yoshimura, and P. Davis, Nat. Photonics, **2**, 728 (2008).
7. I. Kanter, Y. Aviad, I. Reidler, E. Cohen, and M. Rosenbluh, Nat Phot., **4**, 58 (2010).
8. J.-G. Wu, Z.-M. Wu, G.-Q. Xia, T. Deng, X.-D. Lin, X. Tang, and G.-Y. Feng, IEEE Photonics Technol. Lett., **23**, 1854 (2011).
9. S. Y. Xiang, W. Pan, B. Luo, L. S. Yan, X. H. Zou, N. Jiang, N. Q. Li, and H. N. Zhu, IEEE Photonics Technol. Lett., **24**, 1267 (2012).
10. A. Wang, N. Wang, Y. Yang, B. Wang, M. Zhang, and Y. Wang, J. Lightwave Technol., **30**, 3420 (2012).
11. L. Xia, D. Huang, J. Xu, and D. Liu, Opt. Lett., **38**, 3762 (2013).
12. Z. N. Wang, M. Q. Fan, L. Zhang, H. Wu, D. V. Churkin, Y. Li, X. Y. Qian, and Y. J. Rao, Opt. Express, **23**, 15514 (2015).
13. M. Sciamanna and K. A. Shore, Nat Phot., **9**, 151 (2015).
14. A. B. Wang L. S. Wang, P. Li and Y. C. Wang, Opt. Express, **25**, 3153 (2017).
15. M. T. Rosenstein, J. J. Collins, and C. J. Deluca, Phys. D, **65**, 117 (1993).
16. K. Holger, Phys. Lett. A, **185**, 77 (1994).
17. P. Grassberger and I. Procaccia, Phys. D, **9**, 189 (1983).
18. C. Bandt and B. Pompe, Phys. Rev. Lett., **88**, 174102 (2002).
19. M. C. Soriano, L. Zunino, O. A. Rosso, I. Fischer, and C. R. Mirasso, IEEE J. Quantum Electron., **47**, 252 (2011).
20. J. P. Toomey and D. M. Kane, Opt. Express, **22**, 1713 (2014).
21. N. Li, L. Zunino, A. Locquet, B. Kim, D. Choi, W. Pan, and D. S. Citrin, IEEE J. Quantum Electron., **51**, 2200206 (2015).
22. C. Quintero-Quiroz, S. Pigolotti, M. C. Torrent, and C. Masoller, New J. Phys., **17,** 93002 (2015).
23. H. Liu, B. Ren, Q. Zhao, and N. Li, Opt. Commun., 359, 79–84 (2016).
24. D. Rontani, E. Mercier, D. Wolfersberger, and M. Sciamanna, Opt. Lett., **41,** 4637 (2016).
25. N. Oliver, M. C. Soriano, D. W. Sukow, and I. Fischer, Opt. Lett. **23**, 4632 (2011).
26. N. Oliver, M. C. Soriano, D. W. Sukow, and I. Fischer, IEEE J. Quantum Electron., **49**, 910 (2013).
27. R. Lang and K. Kobayashi, IEEE J. Quantum Electron., **16**, 347 (1980).
28. T. Heil, I. Fischer, W. Elsäßer and A. Gavrielides, Phys. Rev. Lett. **87**, 243901 (2001).
29. S. Ji and Y. Hong, IEEE J. Sel. Top. quantum Electron., accepted to be published in Nov./Dec. 2017. DOI: 10.1109/JSTQE.2017.2689328
30. Y. C. Chung and Y. H. Lee, IEEE Photonics Technol. Lett., **3**, 597 (1991).